Petroleum Science 19 (2022) 554–569

Contents lists available at ScienceDirect

Petroleum Science

journal homepage: www.keaipublishing.com/en/journals/petroleum-science

Original Paper

Bedding parallel fractures in fine-grained sedimentary rocks: Recognition, formation mechanisms, and prediction using well log

Jin Lai [a, b, *], Bing-Chang Liu [b], Hong-Bin Li [b], Xiao-Jiao Pang [b], Shi-Chen Liu [b], Meng Bao [b], Gui-Wen Wang [a, b, **]

[a] State Key Laboratory of Petroleum Resources and Prospecting, China University of Petroleum (Beijing), Beijing, 102249, China
[b] College of Geosciences, China University of Petroleum (Beijing), Beijing, 102249, China

ARTICLE INFO

Article history:
Received 26 January 2021
Accepted 21 June 2021
Available online 23 October 2021

Edited by Jie Hao and Teng Zhu

Keywords:
Bedding parallel fracture
Fine-grained sedimentary rocks
Image logs
Lucaogou Formation

ABSTRACT

Core, thin section, conventional and image logs are used to provide insights into distribution of fractures in fine grained sedimentary rocks of Permian Lucaogou Formation in Jimusar Sag. Bedding parallel fractures are common in fine grained sedimentary rocks which are characterized by layered structures. Core and thin section analysis reveal that fractures in Lucaogou Formation include tectonic inclined fracture, bedding parallel fracture, and abnormal high pressure fracture. Bedding parallel fractures are abundant, but only minor amounts of them remain open, and most of them are partly to fully sealed by carbonate minerals (calcite) and bitumen. Bedding parallel fractures result in a rapid decrease in resistivity, and they are recognized on image logs to extend along bedding planes and have discontinuous surfaces due to partly-fully filled resistive carbonate minerals as well as late stage dissolution. A comprehensive interpretation of distribution of bedding parallel fractures is performed with green line, red line, yellow line and blue line representing bedding planes, induced fractures, resistive fractures, and open (bedding and inclined) fractures, respectively. The strike of bedding parallel fractures is coinciding with bedding planes. Bedding parallel fractures are closely associated with the amounts of bedding planes, and high density of bedding planes favor the formation of bedding parallel fractures. Alternating dark and bright layers have the most abundant bedding parallel fractures on the image logs, and the bedding parallel fractures are always associated with low resistivity zones. The results above may help optimize sweet spots in fine grained sedimentary rocks, and improve future fracturing design and optimize well spacing.

1. Introduction

Fine-grained sedimentary rocks, which are deposited in low-energy environments, account for 2/3 of the entire sedimentary sequences, and they are both source rocks and effective reservoirs for unconventional petroleum systems (shale oil and tight oil play) (Aplin and Macquaker, 2011; Liu et al., 2019). The Lucaogou Formation in Jimusar Sag is typical fine-grained sedimentary rocks, of which the lithologies are dominated by dolomitic mudstones, silty mudstones, muddy siltstones, dolomitic siltstone, dolomicrite and dolarenite (Liu et al. 2019, 2020). Recently, abundant unconventional resources have been discovered in the Lucaogou Formation, showing huge potential for tight oil or shale oil exploration and development (Zhang et al. 2017, 2019; Liu et al., 2019).

Fine-grained sedimentary rocks are characterized by layered structures (Gale et al., 2014; Yawar and Schieber, 2017; Li et al., 2018; Ding et al., 2019; Liu et al., 2021). There are many laminas of various thickness and components in fine-grained sedimentary rocks (Yawar and Schieber, 2017; Wang et al., 2019). In addition, the lamina planes or bedding interfaces are favorable for the formation of bedding parallel fractures. Bedding parallel fractures are the breakage of rocks along weak bedding planes (Li et al., 2021). Actually, natural fractures or joints are extremely common in the layered rocks due to fracturing along the multiple weak bedding interfaces (Zeng and Li, 2009; Lee et al., 2015; Chang et al., 2015; Weng et al., 2018; Li et al., 2021). Bedding parallel fractures are known to strongly influence subsurface fluid flow (Swanson et al., 2007; McGinnis et al., 2017; Ladevèze et al., 2018; Basa et al.,

* Corresponding author.
** Corresponding author.
E-mail addresses: laijin@cup.edu.cn (J. Lai), wanggw@cup.edu.cn (G.-W. Wang).

https://doi.org/10.1016/j.petsci.2021.10.017

2019; Liang et al., 2021), and therefore can significantly improve hydrocarbon storage and productivity (Zeng et al., 2016; Zhang et al., 2019; Liu et al., 2020; Ju et al., 2020; Li et al., 2021; Mohammed et al., 2021).

Therefore subsurface fracture prediction using well logs is important in wells lacking core data with the aim to perform a comprehensive fracture characterization (McGinnis et al., 2017; Ladevèze et al., 2018; Xu et al., 2020; Li et al., 2021). However, the prediction of distribution of bedding parallel fractures in the subsurface remains a challenge. Therefore in this study, special aims are paid to unravel the bedding parallel fractures in the Lucaogou Formation in Jimusar Sag. The organizations of this study are as follows: In section 2, the definition of bedding parallel fracture is introduced, then geological settings are briefly described. In section 4, the data and related log dataset are briefly introduced. Then the definition, recognition criteria of bedding parallel fractures as well as the bedding parallel fractures identified from various data are introduced in Section 5. Next the well log responses of various types of geological objects are characterized, and the conventional log as well as image log data are used to express bedding parallel fractures. Section 6 discusses the formation mechanisms of bedding parallel fractures, and the comprehensive interpretations of distribution of bedding parallel fractures using well logs for each well are presented. The results above are hoped to provide insights in the recognition criterion, formation mechanisms, as well as well log recognition and characterization of bedding parallel fractures using well logs in fine-grained sedimentary rocks.

2. Definition of bedding parallel fractures

In geology, fracture is defined as any discontinuity in rocks where cohesions have been lost through a brittle deformation process (Price, 1966; McGinnis et al., 2017). Most rocks are fractured at various scales ranging from micro-, meso-, to macroscales (McGinnis et al., 2017). The complex fracture networks formed by various mechanisms are main pathway for fluid flow, and even determine permeability of reservoir rocks (Momeni et al., 2019; Heng et al., 2020; Liang et al., 2021).

Fractures can be classified as macrofractures and microfractures (aperture<0.1 mm) in terms of core and thin section observation (Anders et al., 2014; Lai et al., 2017). From the aspects of mechanical properties, structural (tectonic) and nonstructural fractures can be divided. The structural fracture includes tension fracture, shear fracture and tension-shear fractures, while nonstructural fracture consist of abnormal high-pressure (hydrocarbon generation) fractures, diagenetic microfracture, etc (Zeng et al., 2016; Zhang et al. 2017, 2019; Gu et al., 2020). Nonstructural fractures also include bedding parallel fractures and interlayer fractures (fractures developed along the lithology interfacies, but not bedding planes) (Gu et al., 2020). Fractures can also be classified into veins (most common vein filling calcite mineral) and unfilled fractures (Basa et al., 2019). Differentiating fractures of various origins using well logs (sonic and image) remain a challenging task, and therefore in terms of well log evaluation, (natural) fractures are commonly classified as vertical fracture, high angle inclined fracture (>60°), medium angle inclined fracture (30–60°), and low angle or horizontal fracture (<30°) (Lai et al., 2017; Basa et al., 2019). Additionally, electrical and sonic image logs can also detect induced fractures and borehole breakouts (Lai et al., 2018).

Bedding parallel fractures are the breakages along stratification or foliation of rocks (Li et al., 2021). Bedding parallel fractures were firstly proposed by Price (1966) as sheeting. Then Nelson (1985) and Zeng and Li (2009) called bedding parallel fractures as unloading fractures and interlayer fractures (Li et al., 2021). Shales consist of multiple weak interfaces between layers, and these weak bedding interfaces are easily opened due to changing of in-situ stress status and/or hydrocarbon charging (Zhang et al., 2017; Tang et al., 2018). Bedding parallel fractures is therefore commonly

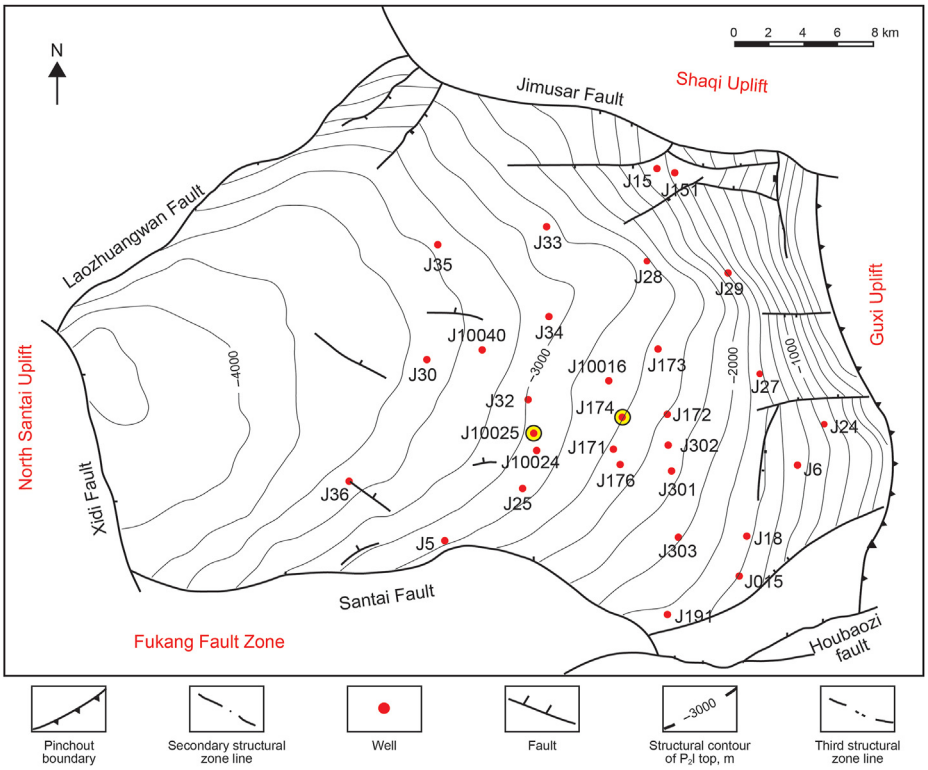

Fig. 1. Map showing structure contour of top of the Lucaogou Formation of the Jimusar Sag in Junggar Basin, West China (S Zhang et al., 2019).

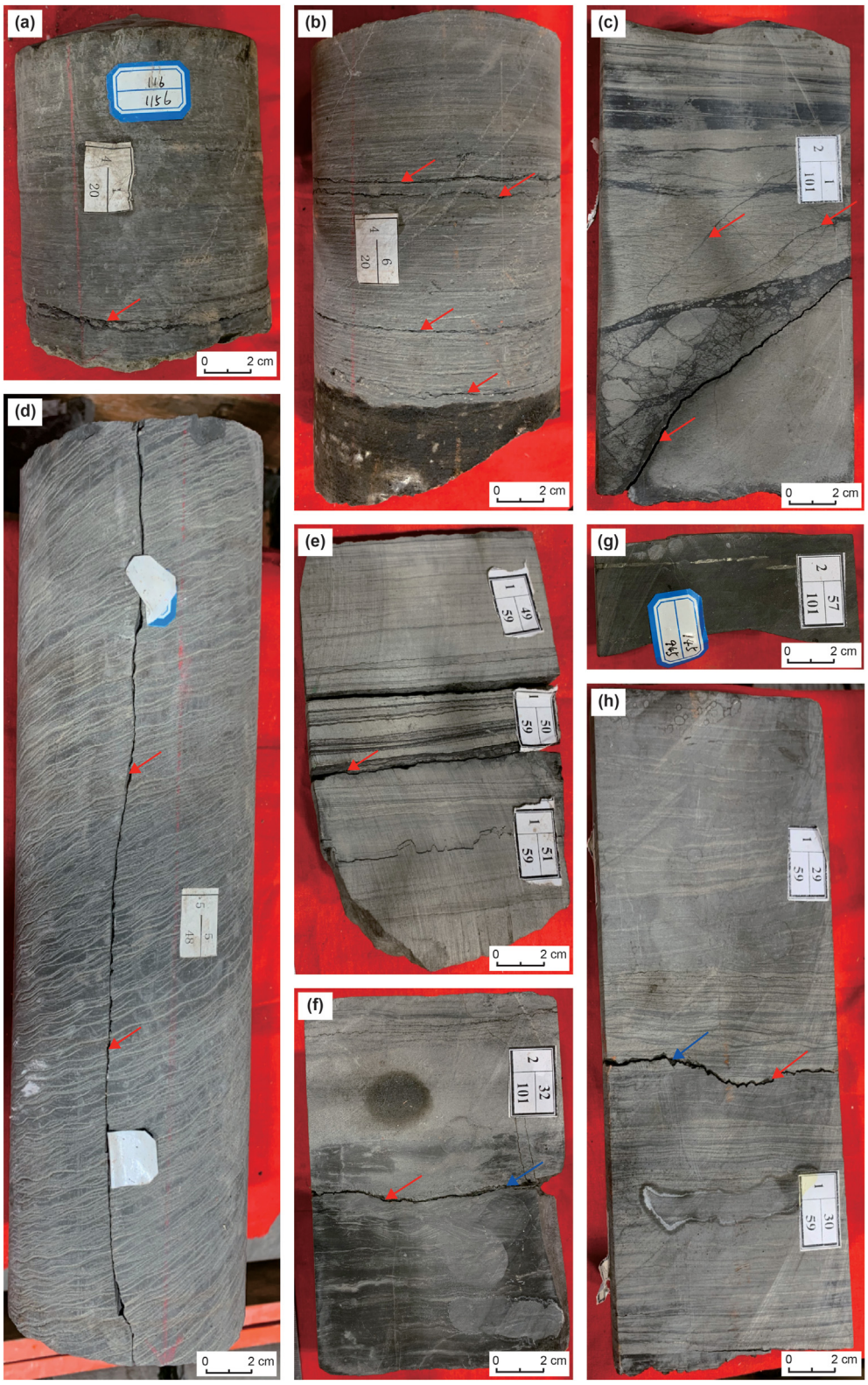

Fig. 2. Core photos show the bedding fractures in Lucaogou Formation, Jimusar Sag. (a). Jagged bedding fractures, J10012, 3293.01m. (b). Three distinct bedding fractures parallel to bedding planes, J10012, 3294.13m. (c). Inclined fractures, J10016. (d). Vertical fractures, J10012. (e). Minerals filling in the bedding planes, J10016. (f). Dissolution and cementation along the bedding surfaces, J10016. (g). Pyrite filling in the bedding planes, J10016. (h). Dissolution and cementation along the bedding surfaces, J10016.

observed in both outcrops and subsurface reservoirs of shale and tight sandstone reservoirs, which are characterized by layered structures (Liu et al., 2020; Li et al., 2021).

3. Geological settings

The Jimusar Sag, which is located in the Junggar Basin, was

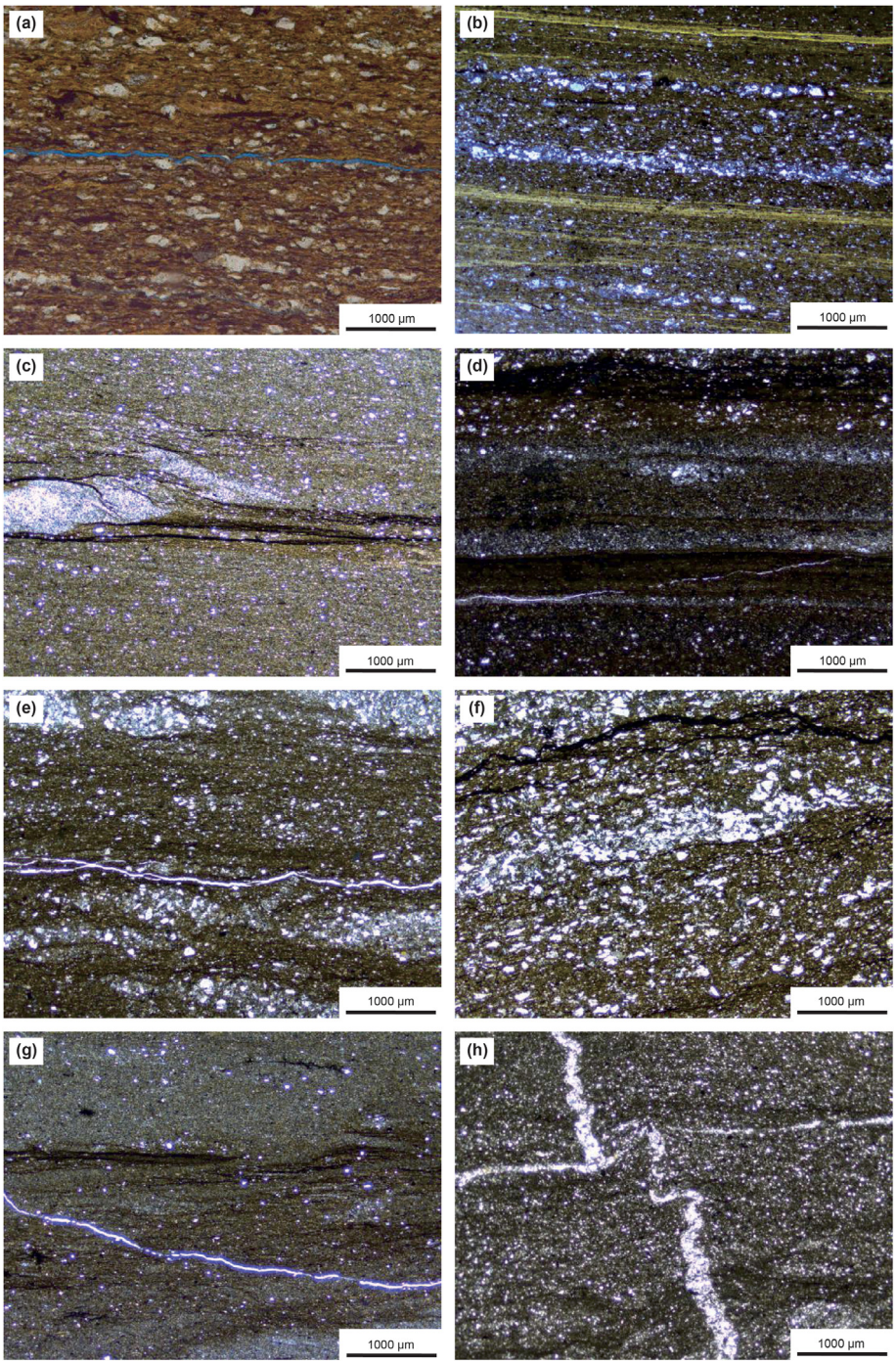

Fig. 3. Thin section images show the bedding fractures in Lucaogou Formation, Jimusar Sag. (a). Micro-fracture parallel to bedding, J176, 3027.29m. (b). Micro-fracture parallel to bedding, J10016, 3310.8m. (c). Filled micro-fractures parallel to bedding planes, J10016, 3311.3m. (d). Half-filled micro-fractures parallel to bedding planes, J251, 3601.065m. (e). Filled micro-fractures parallel to bedding planes, J10016, 3306.3m. (f). Filled micro-fractures parallel to bedding planes, J10016, 3309.2m. (g). Micro-fractures cut through the bedding planes, J10016, 3311.3. (h). Micro-fractures cut through the bedding planes, J10016, 3320.0m.

formed on folded early Carboniferous basement, and has an area of 1300 km^2 (Fig. 1) (Liu et al., 2017; Zhang et al., 2017, 2019; Wang et al., 2020a). Since the late Paleozoic, the Jimusar Sag had experienced multiple stages of tectonic activity, and therefore abundant natural fractures were developed in the Jimusar Sag (Zhang et al., 2017). The Permian Lucaogou Formation (thickness, 200–350m), which was deposited in an evaporative–lacustrine setting (saline lacustrine), is a typical fine-grained sedimentary rock in lacustrine sedimentary sequences (Cao et al., 2017; Zhang et al., 2019; Wang et al., 2020a). The formation is divided into two members, P_2l_1 and P_2l_2, and two sweet spots (porous and permeable reservoirs) are identified in both P_2l_1 and P_2l_2, where commercial oil flow had been obtained from these two subsections (Cao et al., 2017; Zhang et al., 2017). The formation includes a wide range of lithologies (siltstones, mudstones, shales and carbonates) (Wang et al., 2020a).

Fig. 4. Core photos show the abnormal pressure fractures in Lucaogou Formation, Jimusar Sag.

4. Materials and methods

Drilled cores were taken from three key wells (J10025, J10024, J10016) (Fig. 1), and special attentions were paid on the fractures including bedding parallel fractures, structural high or low angle fractures as well as the materials filling in the fractures. Also the aperture, dip angle, and filling degree of fractures were examined.

Thin sections (30 μm in thickness) were cut perpendicular to beddings, and were observed with Leica microscope at the State Key Laboratory of Petroleum Resources and Prospecting under both planar and cross polarized lights (PPL and XPL), with the special aim to highlight the micro-fractures (and related filled cements) parallel to bedding planes.

Conventional well log suits include three porosity logs (bulk density, sonic transit time, and neutron porosity), three lithology logs (natural gamma ray, caliper and spontaneous potential log), and resistivity logs (deep resistivity Rt, shallow resistivity Rxo, invaded zone resistivity RI). Three porosity logs and resistivity logs, which are sensitive for the presences of fractures, are used for recognition of fractures (Lai et al., 2017).

Borehole (Schlumberger's FMI imaging tool) image log data are processed through speed correction, eccentering correction, and static and dynamic normalization, with the aim to generate high resolution (5 mm or 0.2 inch) colorful borehole images (Lai et al., 2018). The color variations of images represent the resistivity fluctuation, which is the complex reflection of lithology and fluid. In the static image, the color range is normalized over the entire interpreted intervals (tens or hundreds of meters), while color range is normalized over only a sliding window (commonly 0.6096 m) (Donselaar and Schmidt, 2005; Wilson et al., 2013; Keeton et al., 2015; Niu et al., 2020; Wang et al., 2020b). Image logs can capture natural fractures as well as dissolution vugs (Aghli et al., 2020; Lai et al., 2020).

Fractures (inclined and bedding parallel), which appeared as evident sinusoidal waves on the images (Lai et al., 2021a), were manually picked out by fitting sinusoidal curves in the Techlog software (Lai et al., 2019). In water based drilling fluids, open fractures appear as dark sinusoidal waves, whereas (calcite) filled fractures are recognized as bright sinusoidal waves (Lai et al., 2019; Liu et al., 2020). Natural fractures were differentiated from induced fractures according to characteristics of crosscutting the wellbores, and 180° apart (Lai et al., 2018; Liu et al., 2020).

5. Results

5.1. Recognition criteria of bedding parallel fractures

Bedding planes are weak interfaces, and the mechanical property of bedding planes is much weaker than rock matrix, therefore failure occurs while the loading stresses exceed the compressive strength of rocks (Gu et al., 2020; Liang et al., 2021). Bedding parallel fracture is one of the most developed nonstructural fractures in fine-grained sedimentary rocks (for instance, shales) (Gu et al., 2020). Therefore the presence of weak bedding interfaces in layered shales favor the fracture growth, and the well-developed bedding planes will be opened to form bedding parallel fractures due to changing of rock mechanics. There are distinct fracture surfaces for bedding parallel fractures (Heng et al., 2020; Liang et al., 2021).

Bedding parallel fracture belongs to nonstructural fracture forming along the bedding surface under the influence of mechanical compaction and weathering (Gu et al., 2020). In Lucaogou

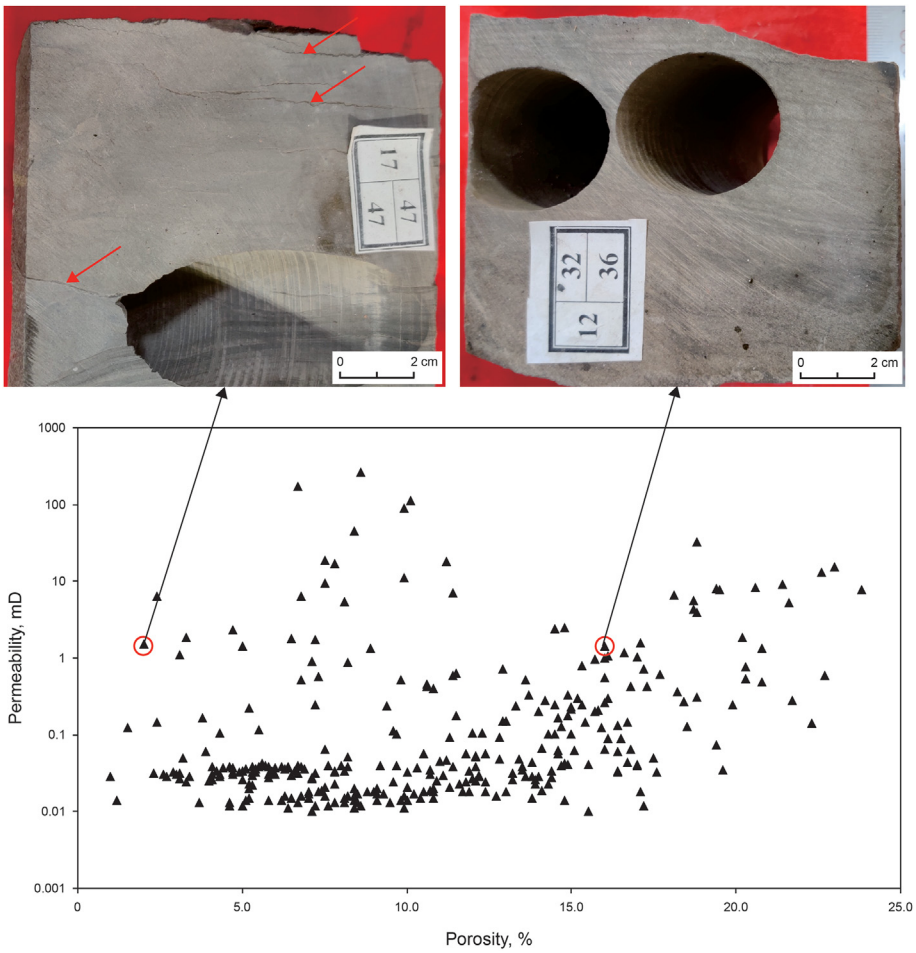

Fig. 5. Core-measured porosity and permeability of Lucaogou Formation in Jimusar Sag.

Formation, the bedding parallel fractures can be differentiated from cross (parallel) bedding planes due to their distinct fracture (discontinuous) surfaces (Fig. 2a and b). Fractures, which are in the direction normal or oblique to bedding planes, are classified as vertical or inclined fractures (Fig. 2c and d). Additionally, there are abnormal high pressure fractures, which are commonly filled by calcite cements, can be detected by core observations (Fig. 2c and d).

Bedding parallel fracture surfaces are commonly filled by quartz or calcite and other minerals (Fig. 2e), additionally, dissolution along fractures can also be detected (Fig. 2f). Sometimes multiple stages of cementation and dissolution along fracture surfaces can be observed simultaneously (Fig. 2g and h). Actually, early filling carbonate and other minerals can also be dissolved due to late-stage diagenetic modifications (Gu et al., 2020). Therefore, the scale and quantity effect of bedding parallel fracture on reservoir quality improvement and hydrocarbon productivity is dependent on the open and closure of bedding parallel fractures, which is influenced by the dissolution and cementation along the fracture planes (Gu et al., 2020). Intersection of bedding parallel fractures with tectonic low-angle fractures is rare.

Bedding parallel fractures break the horizontal weak planes (Zhang et al., 2019), and they will extend along bedding surfaces or at low angles (Liu et al., 2020). Therefore the bedding parallel fractures can be recognized as: 1) parallel to the bedding planes (structural planes often cut through the bedding planes), 2) horizontal or with low dip angles, 3) mineral filling and dissolution along the fracture planes (Fig. 2) (Gu et al., 2020).

5.2. Multi-scale characterization of bedding parallel fractures

The complex fracture networks are widely grown in layered rocks (Heng et al., 2020). Fractures typically span several orders of size magnitude from large-scale (tens of meters to kilometer scale) discontinuities or faults (outcrop, seismic data) to smaller-scale (millimeter, centimeter to meter scale) fractures gathered from wellbores (well logs, cores, borehole image logs), and then to microscopic fractures (thin section) (Berkowitz, 2002; Strijker et al., 2012; Espejel et al., 2020; Zhang et al., 2021). Fracture can be determined from multi-scale datasets (core, thin section, well logs), and the multi-scale natural fracture networks from each scale of observation control rock physical properties (Espejel et al., 2020; Lai et al., 2021b).

Seismic data and outcrop characterize macroscopic faults and fractures. Core and image log identify medium-to small-sized filled and open (conductive) fractures. Thin section, SEM and CT provide insights into microfractures (<0.1 mm) (Lai et al., 2017; Gou et al., 2019; Xu et al., 2020). The laminations or bedding planes are commonly approximately 1.0 mm in thickness (He and Afolagboye, 2018). In this study, only those bedding parallel fractures can be observed at the scales of core and thin section are taken into consideration in terms of well log prediction resolution (Fig. 3),

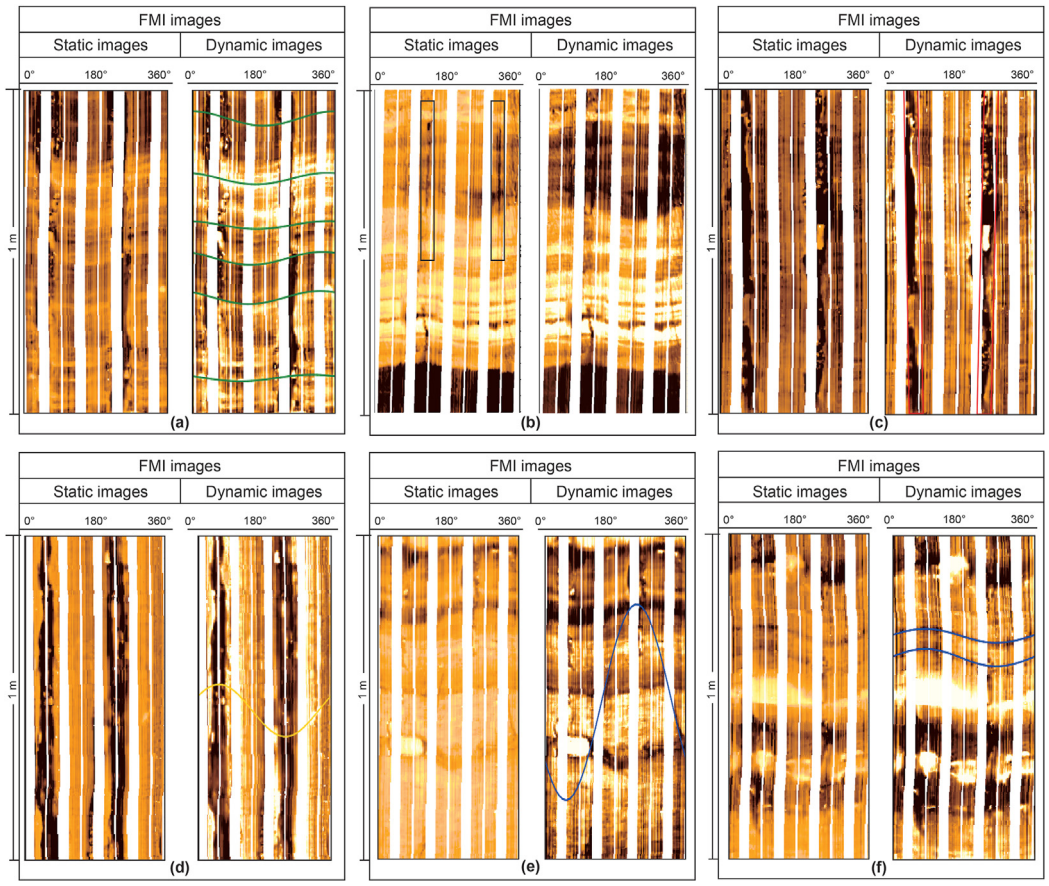

Fig. 6. Capture of geological objects using image logs. (a). Cross bedding picked out as green sinusoidal waves. (b). Induced fractures picked out as black regions. (c). Borehole breakouts picked out as red regions. (d). Resistive fractures picked out as yellow sinusoidal waves. (e). Conductive fractures picked out as blue sinusoidal waves. (f). Bedding parallel fractures picked out as blue sinusoidal waves.

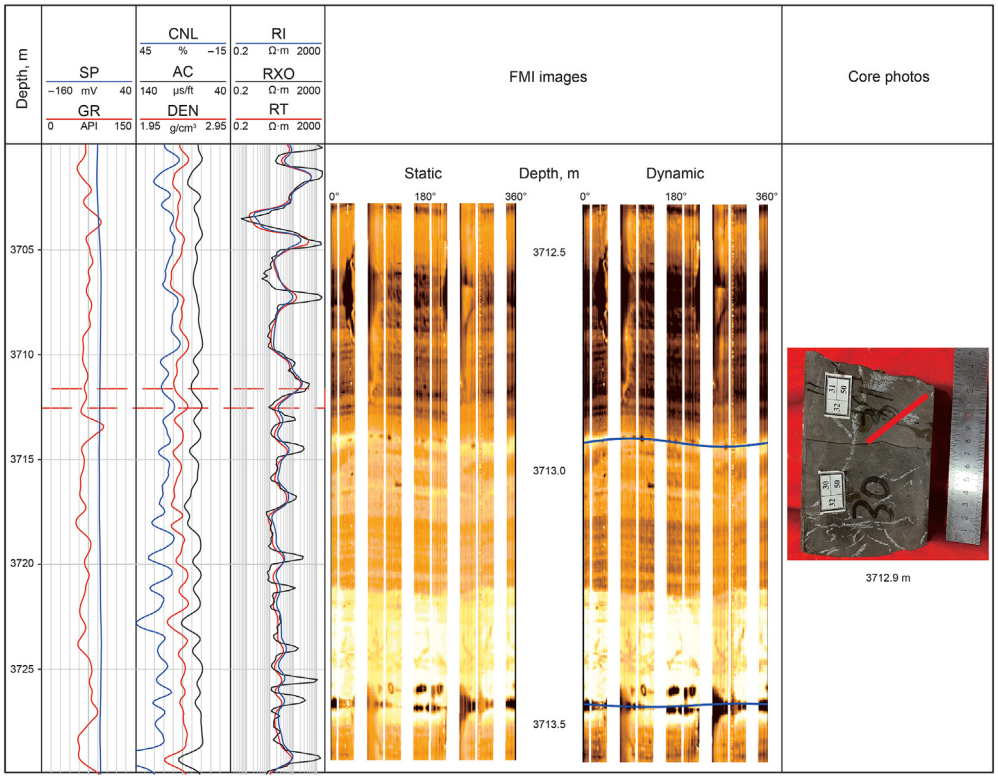

Fig. 7. Image log and conventional well log responses of bedding parallel fractures and abnormal high pressure fractures.
SP: Spontanneous Potential Log, GR: Natural Gamma Ray, CNL: Compensated neutron log, AC: Sonic transit time, DEN: Bulk density, RI: Induced resistivity, Rxo and RT are the shallow and deep resistivity log, and RI is invaded zone resistivity.

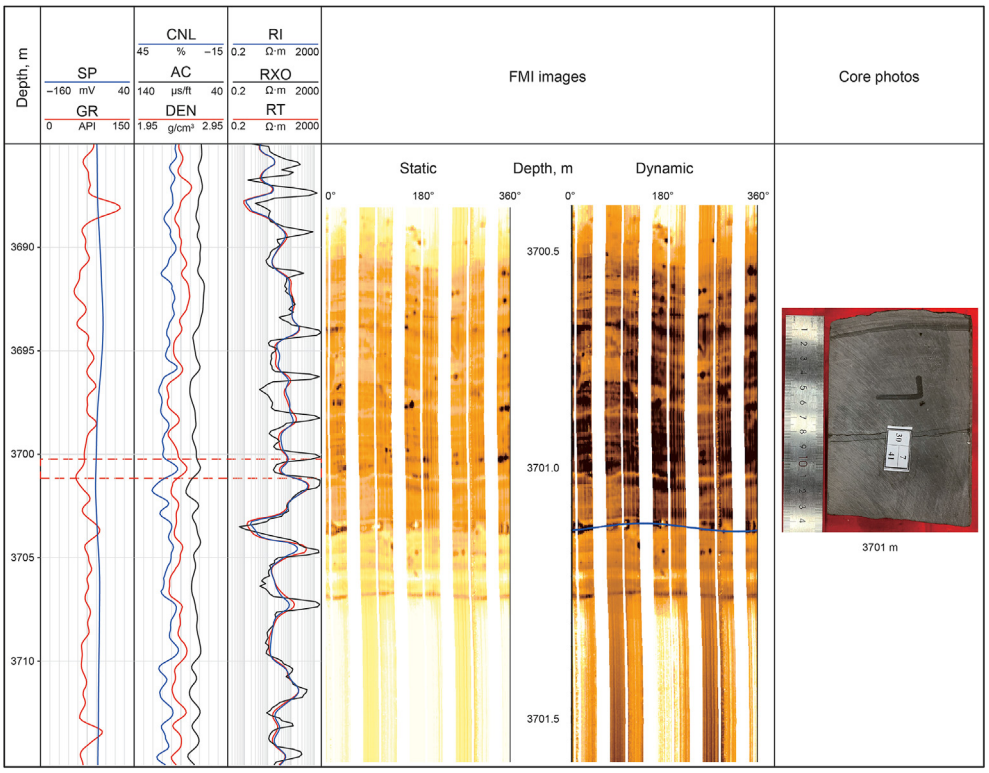

Fig. 8. Conventional and image log expressions of bedding parallel fractures.

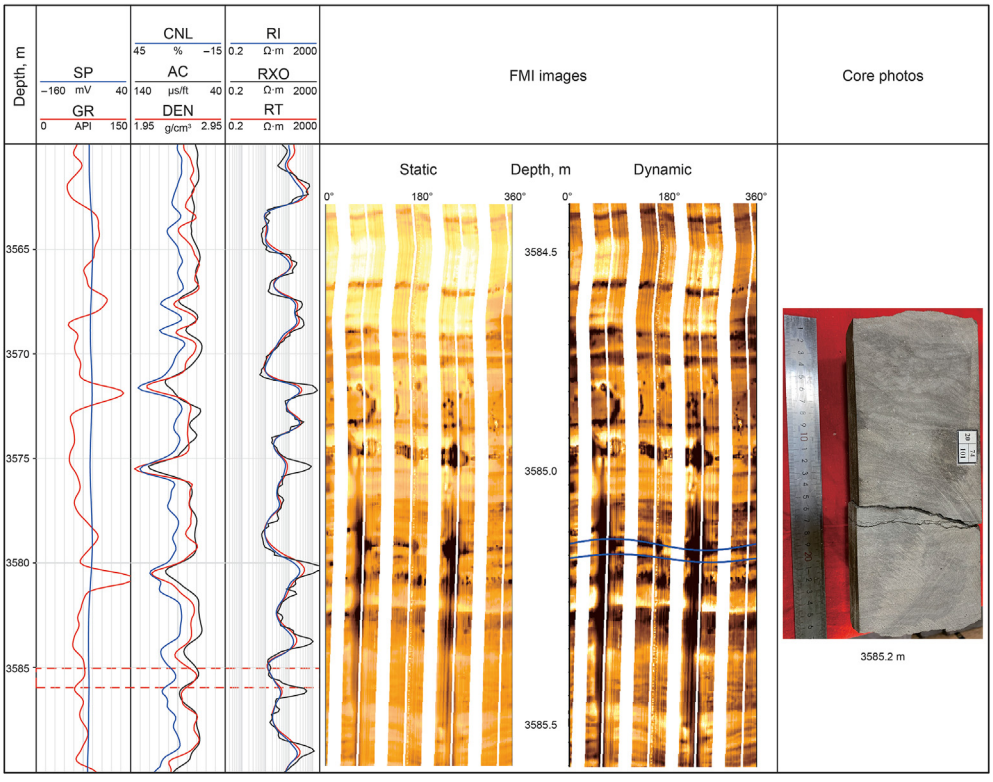

Fig. 9. Response of dissolution and cementation of bedding parallel fractures on conventional and image logs.

while the meter-kilometer scale fractures, which can only be detected by seismic and outcrop, are beyond the scope of this study. At both core and thin section scales of observations, fractures can be correlated with well log data (Fig. 3).

Thin section analysis reveals that bedding parallel micro-fractures are abundant. However, only minor amounts of the micro-fractures remain open (Fig. 3a), while most of them are partly to fully sealed by carbonate minerals (calcite) and bitumen

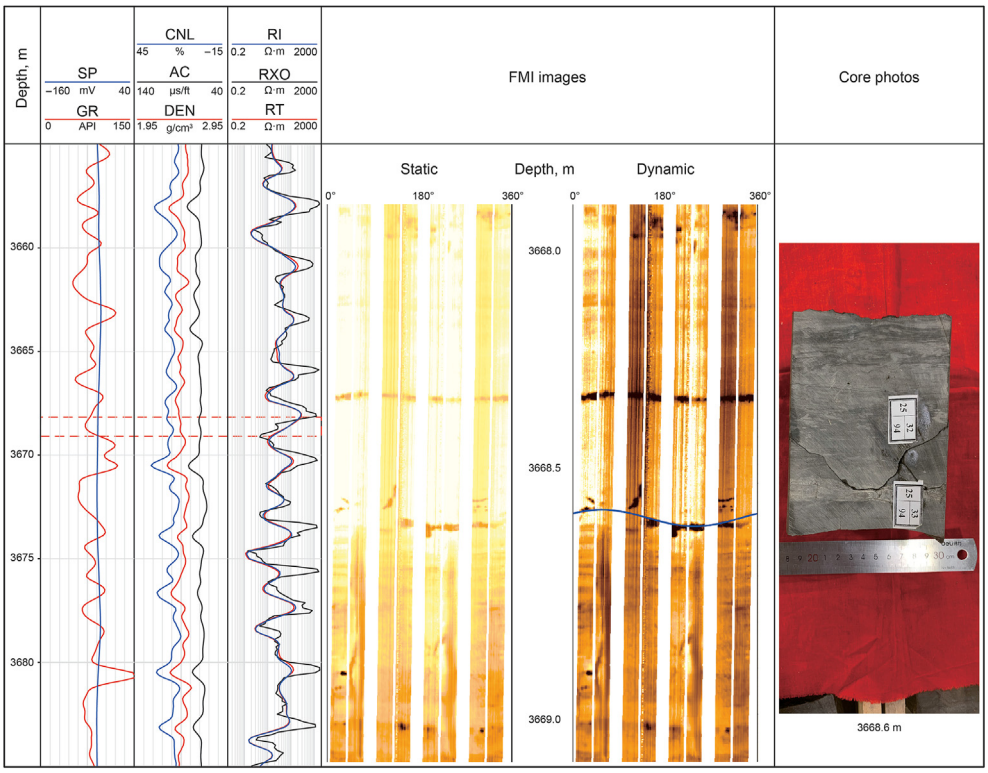

Fig. 10. Conventional and image log expressions of inclined low angle fractures.

(Fig. 3b–e). This is in consistent with the core observation. Also there are also micro-fractures not parallel to the beddings, but cut through the bedding planes (Fig. 3g andh). Micro-fractures fully filled with calcite veins can also be observed (Fig. 3h).

There are also abnormal high-pressure fractures (drainage fractures) developed in the Lucaogou Formation, which are formed by abnormal fluid pressure due to hydrocarbon generation (Zhang et al., 2017; Liu et al., 2020). However, the abnormal fractures in the Lucaogou Formation are commonly fully filled by calcite cements, which are characterized by grouped fracture veins, and therefore they have no contribution to the hydrocarbon productivity (Fig. 4) (Zhang et al., 2019; Liu et al., 2020).

The presences of bedding parallel fractures can also be characterized via appearance of data points characterized with high permeability but low porosity in permeability-porosity crossplot (Fig. 5). Coexistences of (bedding) fractures and various pore spaces in Lucaogou Formation result in the complex fracture networks, which is evidenced by the complex relationships between permeability and porosity (Fig. 5). Cores with bedding parallel fractures, though having low porosity (<5%), can have permeability as high as those samples with porosity higher than 15% (Fig. 5).

5.3. Well log responses

5.3.1. Image log expressions of various geological objects

The whole suite of conventional well logs, which are sensitive for the natural fractures, include caliper (CAL), resistivity logs (Rt, RI, Rxo) and the three porosity logs, especially sonic transit time (AC) (Khoshbakht et al., 2012; Zazoun, 2013; Aghli et al., 2016). Image logs can obtain high resolution (up to 5 mm) “pseudo-picture” of borehole walls (Lai et al., 2021a). Therefore image logs are widely used for subsurface fracture detection and evaluation (Khoshbakht et al., 2009; Ameen et al., 2014; Lai et al. 2018, 2021b). Cross beddings (Fig. 6a), induced fractures (Fig. 6b) and borehole breakouts (Fig. 6c), as well as natural fractures (inclined and bedding parallel) (Fig. 6d, 6e, 6f) are easily recognized on the image logs (Lai et al., 2018; Xu et al., 2020).

Cross bedding appears on image logs as dark and bright sinusoidal waves, in which the lowest points and the amplitudes reflect the dip directions and magnitudes (Folkestad et al., 2012; Lai et al., 2018; Nian et al., 2018). Cross beddings, which can be well imaged on both static and dynamic displays due to the high resistivity contrast (Xu et al., 2015), are picked out as green sinusoidal lines (Fig. 6a).

Drilling-induced (tensile- or shear-induced) fractures are open mode fractures, which are recognized as two vertical fractures on images oriented at 180° from each other or en-echelon fractures (Fig. 6b) (Brudy and Zoback, 1999; Nian et al., 2016), and they are formed due to stress readjustment during drilling. Drilling induced fractures are parallel to in-situ SH_{max} (maximum horizontal stress) orientation (Fig. 6b) (Bell and Gough, 1979; Rajabi et al., 2010; Wilson et al., 2015).

Breakouts are wellbore enlargements, and are broad, parallel, dark bands separated by 180° on image logs. Borehole breakouts appear as 90° in trend from the vertical drilling induced fractures (Fig. 6c), and breakouts indicate minimum horizontal stress (SH_{min}) directions (Bell and Gough, 1979; Ameen, 2014; Nian et al., 2016). Breakouts will not coexist with drilling induced fractures at certain log intervals, however, the in-situ stress direction determined from induced fractures and borehole breakouts commonly coincides with each other (Fig. 6b and c).

Natural high angle fractures intersect with the cross bedding planes and are recognized as dark and bright sinusoidal lines with certain dip angles, providing that they are open and filled with resistive cements (calcite, dolomite, etc) (Fig. 6d and e) (Lai et al.,

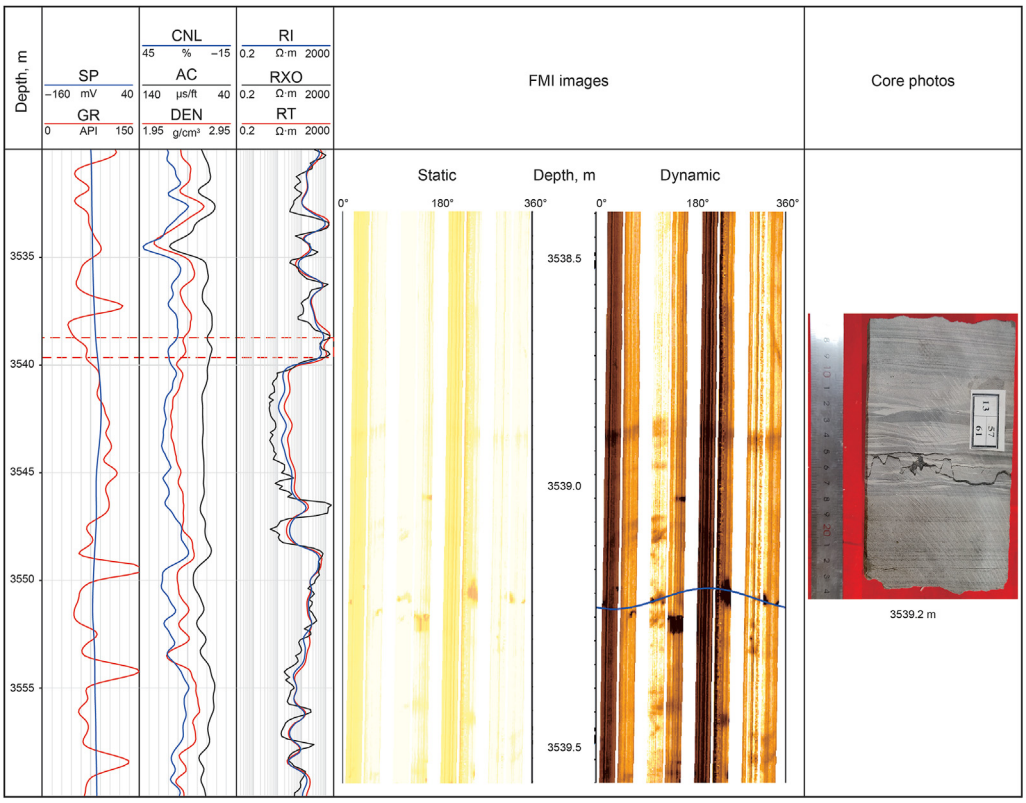

Fig. 11. Recognition of stylolite on conventional and image logs.

2019; Nian et al., 2021). Natural fractures are actually recognized as continuous or discontinuous conductive, resistive, or mixed (partly open and partly filled) sinusoidal waves on the image logs, and they generally cross cut the bedding planes (Fig. 6d and e) (Lai et al., 2018). Resistive and conductive fractures are picked out as yellow and blue sinusoidal lines, respectively (Fig. 6d and e). Fracture attributes in terms of fracture dip direction, dip angle, as well as fracture parameters can be derived from image logs (Nian et al., 2017; Lai et al., 2018; Liu et al., 2020).

Bedding parallel fractures break along the weak planes in horizontal (Zhang et al., 2019). Therefore the bedding parallel fractures are recognized on image logs to extend along bedding planes and have discontinuous surfaces due to partly-fully filled resistive carbonate minerals as well as late stage dissolution (Fig. 6f) (Liu et al., 2020). In contrast, the bedding planes are recognized as continuous dark/bright sinusoidal waves (Fig. 6a).

5.3.2. *Well log expressions of bedding parallel fractures*

Unlike tectonic inclined fractures, the bedding parallel fractures are often discontinuous, without intersecting bedding planes (Fig. 6f). Therefore the bedding parallel fractures are commonly parallel to the bedding planes without communication with each other, and discontinuous surfaces are generally encountered due to dissolution and cementation along the bedding planes (Fig. 7) (Li et al., 2021). In some cases, the bedding parallel fractures will be cross-cut by the abnormal high pressure fractures (Fig. 7). Presences of bedding parallel fractures will result in a rapid decrease of resistivity log values due to the drilling muds invaded in the fracture surfaces (Fig. 7). However, the three porosity logs have no evident responses for the bedding parallel fractures.

Bedding parallel fractures are always developed along the preexisting weak bedding surfaces, and the contact surfaces between lithology also favor the formation of bedding parallel fractures (Fig. 8). As is known, bedding parallel fracture planes are also migration channels for fluids, and therefore the partly dissolution along bedding planes is common. Consequently, the discontinuous planes will be formed, and the image logs will appear as vuggy sinusoidal waves (Fig. 8).

Occasionally, two sets of bedding parallel fractures can be detected, and one of them is kept open, while the other is sealed (Fig. 9). Image logs can easily differentiate the open and closure status of bedding parallel fractures (Fig. 9). The sinusoidal waves reveal that the two fractures are bedding parallel fractures, but only one of them is kept open, and complete sinusoidal wave can be picked out, while the other is sealed, and therefore only very weak sinusoidal wave traces can be picked out (Fig. 9). Conventional well log suits are not sensitive to the presence of bedding parallel fractures, besides the decrease of resistivity log values (Fig. 7–9).

It is worth mentioning that the bedding parallel fractures are of low fracture aperture (<100 μm) due to the overburden rock stress, therefore those dark bands on image logs are not bedding parallel fractures (Fig. 10). Additionally, bedding parallel fractures are of very low dip angles (<10°), and fractures which are not parallel to the bedding planes should be classified as tectonic inclined fractures (Fig. 10).

There is another type of geological objects, i.e., stylolite, which show similar appearances with bedding parallel fractures. However, they can be differentiated from bedding parallel fractures via the serrated surfaces by core observations and jagged image log responses (Fig. 11).

Bedding parallel fractures therefore can be picked out on the image logs according to their fracture surfaces within the bedding planes, discontinuous vuggy fracture surfaces, and the decrease in resistivity values (Fig. 7–9). In addition, bedding parallel fractures

can be differentiated from inclined fractures and stylolite due to the high dip angles of inclined tectonic fractures and serrated surfaces of stylolite (Fig. 10–11). Noting that cores are easily to be fractured or lost along the bedding planes, and actually the heavily fractured zones of core are likely to be lost in drilling (Swanson et al., 2007). Therefore some core interfaces are probably the bedding parallel fractures which are broken during core-taking process. Consequently, some bedding parallel fractures are only observed on image logs, but are not detected by core observations. Actually, image logs can pick out much more bedding parallel fractures that those recognized by core observation (Fig. 7–11).

6. Discussion

6.1. Prediction of bedding parallel fractures using well logs

6.1.1. Beddings and bedding parallel fractures

With green line, red line, yellow line and blue line representing bedding plane, induced fracture, resistive fracture, and open (bedding and inclined) fracture, respectively, a comprehensive interpretation of distribution of bedding parallel fractures using well logs can be processed (Fig. 12). As can be presented in Fig. 12, the bedding parallel fractures are always coexisting with layers with abundant bedding planes (Fig. 12). At certain stress, the bedding planes can be fractured due to release of tectonic stress, conversely, the massive rocks are not easily to form bedding parallel fractures (Fig. 12).

Strata consisting of interbedded brittle and ductile rocks, which are characterized by bright and dark bands/layers on the image logs, are easily to be fractured along the bedding layer, forming bedding parallel fractures (Fig. 12). Actually, the thin shale layers formed by deposition, which appear as alternating dark and bright features on image logs, have consistent appearances with bedding planes (Xu et al., 2020). Bedding parallel fractures usually have narrow openings and are often filled with resistive minerals (calcite and quartz) or conductive minerals (pyrite) (Xu et al., 2020). Massive fine-grained sedimentary rocks (no beddings) generally have no evident bedding parallel fractures (Fig. 12).

6.1.2. Distribution of bedding parallel fractures

Bedding parallel fractures are mainly distributed with the low resistivity intervals (Fig. 7–9). The distribution of bedding parallel fractures in single well shows that low resistivity zones are commonly associated with the bedding parallel fractures (Fig. 13-Fig. 15). The high resistivity zones (corresponding to the bright bands on the image logs) generally contain no bedding parallel fractures. In contrast, the yellow-dark zones on the image logs contain abundant bedding parallel fractures which are picked out as blue sinusoidal lines. Especially, interbedded brittle and ductile rocks, which are corresponding to the alternating dark and bright

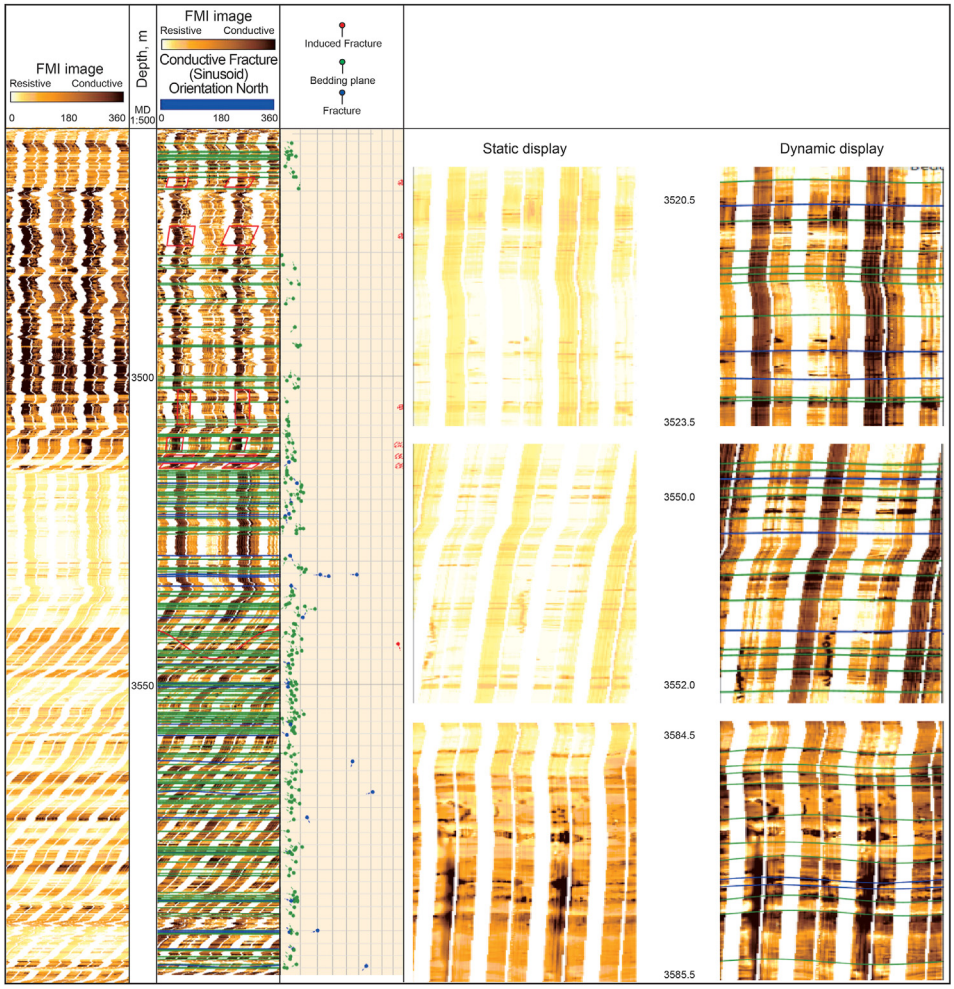

Fig. 12. Relationships between bedding parallel fractures and cross beddings.

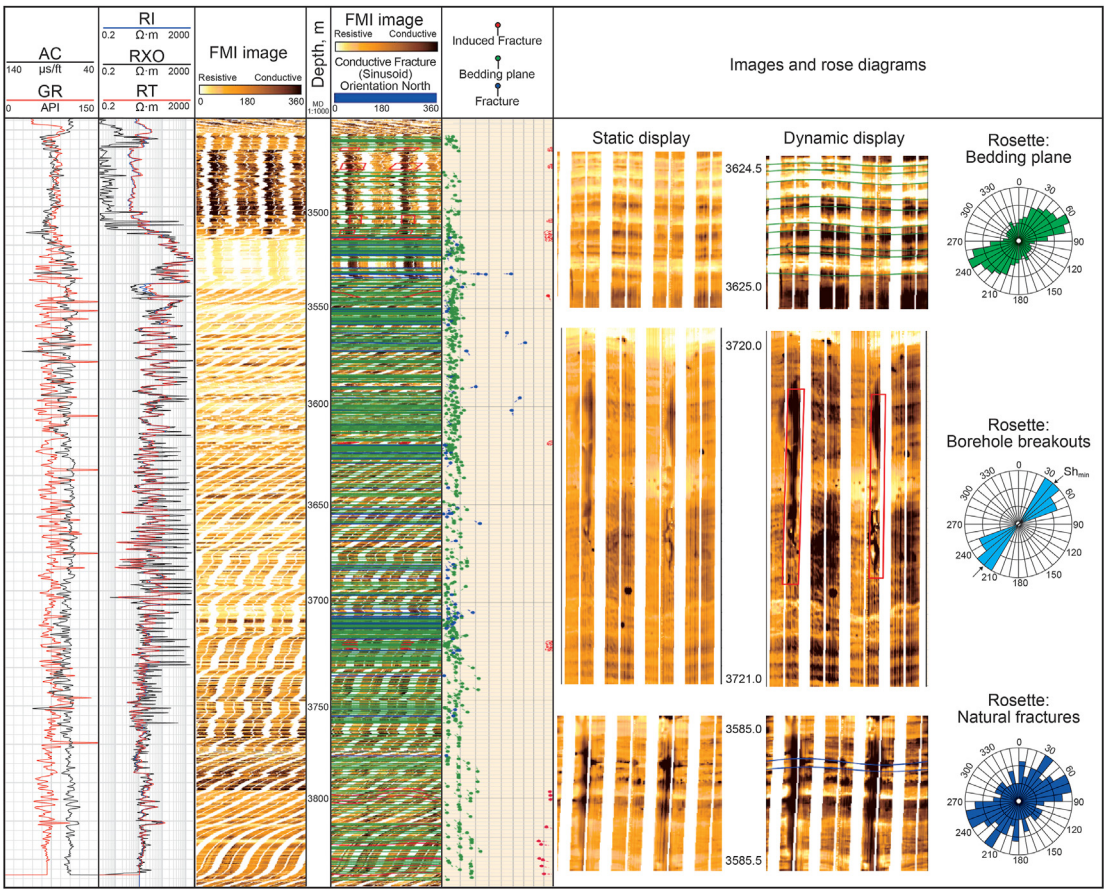

Fig. 13. Distribution of various types of fractures (inclined fractures, bedding parallel fracture, induced fracture and breakouts) and beddings in single well. Note that both the bedding planes and natural fractures have NE-SW strikes.

bands on image logs, have the greatest number of bedding parallel fractures (Fig. 13–15).

The comprehensive evaluation of natural (bedding parallel) fractures, borehole breakouts, induced fractures and bedding planes using image logs for the three wells are presented in Figs. 13–15. The bedding parallel fractures have a broad distribution with depth intervals, and they are closely associated with the bedding planes (red lines). The picked out bedding parallel fractures (blue tadpole plot and rose diagrams) and bedding planes (green tadpole plot and rose diagrams) show that the strike of bedding parallel fractures are closely consistent with the bedding planes (Fig. 13–15). In Fig. 12, the bedding planes have dominant NE-SW strikes, while the strikes of natural bedding parallel fractures are also dominantly NE-SW. This trend can also be observed in both Fig. 14 and Fig. 15. The presences of bedding parallel fractures enhance hydrocarbon productivity significantly. As can be observed in Fig. 13, the intervals from 3540.5 to 3544.5 m contain about 10 fractures, and seven of them are bedding parallel fractures (<10°). A daily oil production of 12.55 ton has been obtained after hydraulic fracturing (cumulative oil production of 287.13 t) (Fig. 13).

Two set of natural fractures, and one of them have NE-SW strikes, which are consistent with bedding planes.

To conclude, bedding parallel fractures are closely associated with the bedding planes, and high density of bedding planes favor the formation of bedding parallel fractures (Fig. 12). The strike of bedding parallel fractures is coinciding with the bedding planes (Fig. 13). Additionally, the bedding parallel fractures are always associated with low resistivity zones, and alternating dark and bright layers on the image logs have the most abundant bedding parallel fractures (Fig. 14–15).

Two sets of natural fractures, and one of them have NE-SW strikes, which are consistent with bedding planes.

6.2. Formation mechanisms

Previous studies show fractures are always initiated in stiffer layers and arrested at bedding planes, in addition, new fractures can initiate along the bedding planes, thus forming layered crumbling rocks (bedding parallel fractures) (Helgeson and Aydin, 1991; Gale et al., 2014; Chang et al., 2020). The formation mechanisms of bedding parallel fractures include external tectonic factors (tectonic stresses) and internal nontectonic origins (Zhang et al., 2019; Gu et al., 2020).

Tectonic stress will concentrate on the weak structural surfaces, which makes it easier to form fractures. Rock begins to fracture when the tectonic stress is greater than the fracture strength (Gu et al., 2020). The presence of bedding planes can lead to a remarkable mechanical behavior of the fine-grained rocks (shales) (Heng et al., 2020). The bedding discontinuities in layered rocks, which are formed in the process of deposition (internal nontectonic origins), are burden by overlying sediments, and this will result in loading pressure. Therefore the bedding parallel fractures would be generated along weak bedding planes if the loading pressure was released during tectonic uplifting and erosion

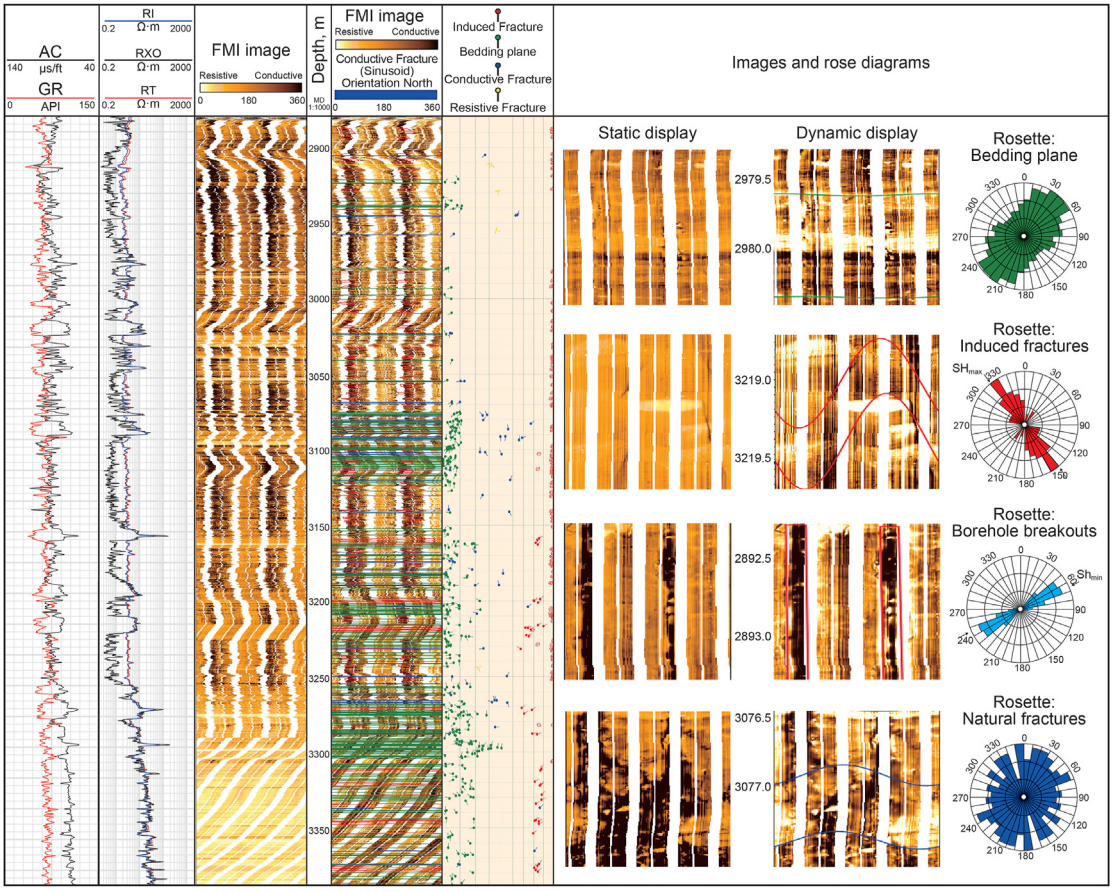

Fig. 14. Comprehensive evaluation of natural (bedding parallel) fractures, borehole breakouts, induced fractures and bedding planes using image logs (J10020).

(changing of external tectonic factors) (Dewhurst et al., 2011; Zhang et al. 2017, 2019). However, the persistent overburden pressure will result in a low aperture of bedding parallel fracture (Fig. 7–9). Additionally, dehydration of clay minerals during diagenetic evolution, intrusion of overpressured fluids generated by thermal evolution of organic matters, will also result in intraparticle fractures fracturing (Zhang et al., 2019; Liu et al., 2020). Actually, overpressured fluids due to hydrocarbon generation will lead the bedding parallel fractures to open up (Zhang et al., 2017).

The internal origins of bedding parallel fracture formation also include the interlayers between various lithofacies. The lithologically weak contact surfaces are commonly rich in carbonaceous or quartz cements, which imply rapid change of rock composition mechanical properties, and therefore they can be opened due to changing of tectonic stress (Swanson et al., 2007; Zhang et al., 2017; Li et al., 2021). Horizontal fractures are easily developed at transition contacts from one lithofacies to another (Swanson et al., 2007). Dissolution along fracture surfaces improves fracture connectivity, especially the secondary fracture fills are dissolved, the fracture connectivity and effectiveness will be enhanced (Fig. 7–9) (Zhang et al., 2017). However, bedding parallel fracture aperture is commonly lower than those high angle fractures due to overburden pressure (Li et al., 2021).

To conclude, both sedimentation and tectonism play important roles in controlling bedding parallel fracture formation in the Lucaogou Formation (Li et al., 2021). Abundant laminas will be formed in the process of deposition due to climate change and source supply (Zeng et al., 2016). Bedding parallel fracture forms along the depositional process controlling weakness plane under the effect of tectonic stress (Zeng and Li, 2009; Li et al., 2021). Additionally, the diagenetic modifications occurred shortly after deposition, deep burial, and uplift could give rise to bedding parallel fractures in Lucaogou Formation (Gale et al., 2014). Additionally these diagenetic modifications include dry shrinkage (forming shrinking bedding fractures), mineral transformation, weathering and high pressure due to hydrocarbon generation (Gou et al., 2019; Heng et al., 2020).

7. Conclusions

Natural fractures in Lucaogou Formation include tectonic inclined fracture, bedding parallel fracture, and abnormal high pressure fracture. Bedding parallel fractures are always developed along the preexisting weak bedding surfaces, and the presence of bedding planes as well as contact surfaces between lithology also favor the formation of bedding parallel fractures.

Bedding parallel fractures have low fracture aperture, and only minor amounts of them remain open, and most of them are partly to fully sealed by carbonate minerals (calcite) and bitumen. Bedding parallel fractures will result in a rapid decrease in resistivity, and they are recognized on the image logs to extend along bedding planes and have discontinuous surfaces due to partly-fully filled resistive carbonate minerals as well as late stage dissolution.

The strike of bedding parallel fractures is coinciding with the bedding planes. Bedding parallel fractures are determined by the amounts of bedding planes, and high density of bedding planes

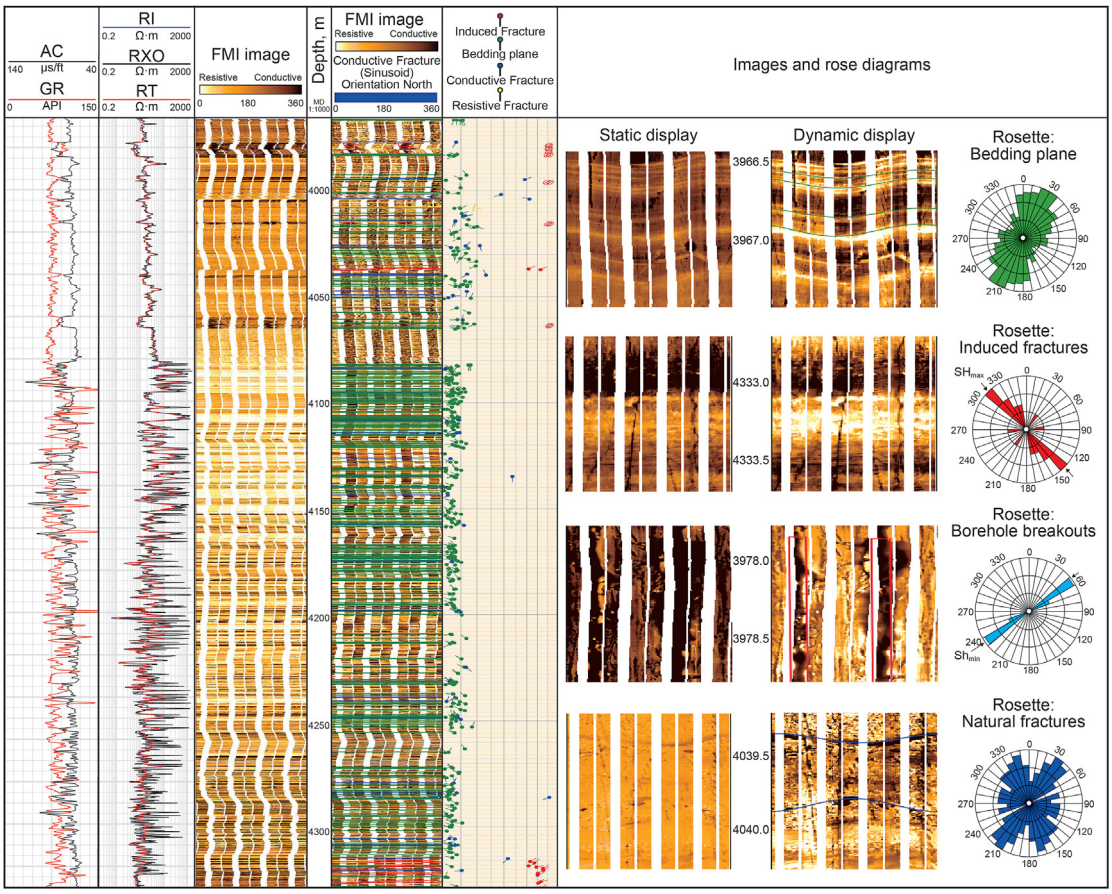

Fig. 15. Prediction of natural (bedding parallel) fractures, borehole breakouts, induced fractures and bedding planes using image logs (J10060).

favor the formation of bedding parallel fractures. Alternating dark and bright layers have the most abundant bedding parallel fractures on the image logs.

Acknowledgments

We thank PetroChina Xinjiang Oilfield Company for providing samples and data access. This work is financially supported by the National Natural Science Foundation of China (No. 42002133, 42072150), Natural Science Foundation of Beijing (8204069), Strategic Cooperation Project of PetroChina and CUPB (ZLZX2020-01-06-01) and Science Foundation of China University of Petroleum, Beijing (No. 2462021YXZZ003). We are also grateful to the four reviewers, whose comments improved the manuscript.

References

Aghli, G., Moussavi-Harami, R., Mohammadian, R., 2020. Reservoir heterogeneity and fracture parameter determination using electrical image logs and petrophysical data (a case study, carbonate Asmari Formation, Zagros Basin, SW Iran). Petrol. Sci. 17, 51–69. https://doi.org/10.1007/s12182-019-00413-0.

Aghli, G., Soleimani, B., Moussavi-Harami, R., et al., 2016. Fractured zones detection using conventional petrophysical logs by differentiation method and its correlation with image logs. J. Petrol. Sci. Eng. 142, 152–162. https://doi.org/10.1016/j.petrol.2016.02.002.

Ameen, M.S., 2014. Fracture and in-situ stress patterns and impact on performance in the khuff structural prospects, eastern offshore Saudi Arabia. Mar. Petrol. Geol. 50 (50), 166–184. https://doi.org/10.1016/j.marpetgeo.2013.10.004.

Anders, M.H., Laubach, S.E., Scholz, C.H., 2014. Microfractures: a review. J. Struct. Geol. 69 (Part B), 377–394. https://doi.org/10.1016/j.jsg.2014.05.011.

Aplin, C.A., Macquaker, H.I.S., 2011. Mudstone diversity: origin and implications for source, seal, and reservoir properties in petroleum systems. AAPG (Am. Assoc. Pet. Geol.) Bull. 95 (12), 2031–2059. https://doi.org/10.1306/03281110162.

Basa, A., Ahmed, F., Bhattacharyya, K., et al., 2019. Evolution and characterization of fracture patterns: insights from multi-scale analysis of the Buxa dolomite in the Siang Valley, Arunachal Lesser Himalayan fold-thrust belt. J. Struct. Geol. 123, 54–66. https://doi.org/10.1016/j.jsg.2019.03.004.

Bell, J.S., Gough, D.I., 1979. Northeast-southwest compressive stress in Alberta: evidence from oil wells. Earth Planet Sci. Lett. 45 (2), 475–482. https://doi.org/10.1016/0012-821X(79)90146-8.

Berkowitz, B., 2002. Characterizing flow and transport in fractured geological media: a review. Adv. Water Resour. 25 (8e12), 861–884. https://doi.org/10.1016/S0309-1708(02)00042-8.

Brudy, M., Zoback, M.D., 1999. Drilling-induced tensile wall-fractures: implications for determination of in-situ orientation and magnitude. Int. J. Rock Mech. Min. Sci. 36 (2), 191–215. https://doi.org/10.1016/S0148-9062(98)00182-X.

Chang, X., Shan, Y., Zhang, Z., et al., 2015. Behavior of propagating fracture at bedding interface in layered rocks. Eng. Geol. 197, 33–41. https://doi.org/10.1016/j.enggeo.2015.08.010.

Chang, X., Zhao, H., Cheng, L., 2020. Fracture propagation and coalescence at bedding plane in layered rocks. J. Struct. Geol. 141, 104213. https://doi.org/10.1016/j.jsg.2020.104213.

Cao, Z., Liu, G., Zhan, H., et al., 2017. Geological roles of the siltstones in tight oil play. Mar. Petrol. Geol. 83, 333–344. https://doi.org/10.1016/j.marpetgeo.2017.02.020.

Dewhurst, D.N., Siggins, A.F., Sarout, J., et al., 2011. Geomechanical and ultrasonic characterization of a Norwegian Sea shale. Geophysics 76 (3), WA101–WA111. https://doi.org/10.1190/1.3569599.

Ding, L., Wang, Z., Liu, B., et al., 2019. Borehole stability analysis: a new model considering the effects of anisotropic permeability in bedding formation based on poroelastic theory. J. Nat. Gas Sci. Eng. 69, 102932. https://doi.org/10.1016/j.jngse.2019.102932.

Donselaar, M.E., Schmidt, J.M., 2005. Integration of outcrop and borehole image logs for high-resolution facies interpretation: example from a fluvial fan in the Ebro Basin, Spain. Sedimentology 52, 1021–1042. https://doi.org/10.1111/j.1365-3091.2005.00737.x.

Espejel, R.L., Alves, T.M., Blenkinsop, T.G., 2020. Multi-scale fracture network characterisation on carbonate platforms. J. Struct. Geol. 140, 104160. https://doi.org/10.1016/j.jsg.2020.104160.

Folkestad, A., Veselovsky, Z., Roberts, P., 2012. Utilising borehole image logs to interpret delta to estuarine system: a case study of the subsurface Lower

Jurassic Cook Formation in the Norwegian northern North Sea. Mar. Petrol. Geol. 29 (1), 255–275. https://doi.org/10.1016/j.marpetgeo.2011.07.008.
Gale, J.F.W., Laubach, S.E., Olson, J.E., et al., 2014. Natural fractures in shale: a review and new observations. AAPG (Am. Assoc. Pet. Geol.) Bull. 98 (11), 2165–2216. https://doi.org/10.1306/08121413151.
Gou, Q., Xu, S., Hao, F., et al., 2019. Full-scale pores and micro-fractures characterization using FE-SEM, gas adsorption, nano-CT and micro-CT: a case study of the Silurian Longmaxi Formation shale in the Fuling area, Sichuan Basin, China. Fuel 253, 167–179. https://doi.org/10.1016/j.fuel.2019.04.116.
Gu, Y., Ding, W., Tian, Q., et al., 2020. Developmental characteristics and dominant factors of natural fractures in lower Silurian marine organic-rich shale reservoirs: a case study of the Longmaxi formation in the Fenggang block, southern China. J. Petrol. Sci. Eng. 192, 107277. https://doi.org/10.1016/j.petrol.2020.107277.
He, J., Afolagboye, L.O., 2018. Influence of layer orientation and interlayer bonding force on the mechanical behavior of shale under Brazilian test conditions. Acta Mech. Sin. 34 (2), 349–358. https://doi.org/10.1007/s10409-017-0666-7.
Heng, S., Li, X., Liu, X., et al., 2020. Experimental study on the mechanical properties of bedding planes in shale. J. Nat. Gas Sci. Eng. 76, 103161. https://doi.org/10.1016/j.jngse.2020.103161.
Helgeson, D.E., Aydin, A., 1991. Characteristics of joint propagation across layer interfaces in sedimentary rocks. J. Struct. Geol. 13 (8), 897–911. https://doi.org/10.1016/0191-8141(91)90085-W.
Ju, W., You, Y., Feng, S., et al., 2020. Characteristics and genesis of bedding-parallel fractures in tight sandstone reservoirs of Chang 7 oil layer, Ordos Basin. Oil Gas Geol. 41 (3), 596–605. https://doi.org/10.11743/ogg20200315 in Chinese.
Keeton, G., Pranter, M., Cole, R.D., et al., 2015. Stratigraphic architecture of fluvial deposits from borehole images, spectral-gamma-ray response, and outcrop analogs, Piceance Basin, Colorado. AAPG (Am. Assoc. Pet. Geol.) Bull. 99 (10), 1929. https://doi.org/10.1306/05071514025, 1956.
Khoshbakht, F., Memarian, H., Mohammadnia, M., 2009. Comparison of Asmari, Pabdeh and Gurpi formation's fractures, derived from image log. J. Petrol. Sci. Eng. 67, 65–74. https://doi.org/10.1016/j.petrol.2009.02.011.
Khoshbakht, F., Azizzadeh, M., Memarian, H., et al., 2012. Comparison of electrical image log with core in a fractured carbonate reservoir. J. Petrol. Sci. Eng. 289–296. https://doi.org/10.1016/j.petrol.2012.03.007, 86–87.
Ladevèze, P., Séjournéc, S., Rivardb, C., et al., 2018. Defining the natural fracture network in a shale gas play and its cover succession: the case of the Utica Shale in eastern Canada. J. Struct. Geol. 108, 157–170. https://doi.org/10.1016/j.jsg.2017.12.007.
Lai, J., Wang, G., Fan, Z., et al., 2017. Fracture detection in oil-based drilling mud using a combination of borehole image and sonic logs. Mar. Petrol. Geol. 84, 195–214. https://doi.org/10.1016/j.marpetgeo.2017.03.035.
Lai, J., Wang, G., Wang, S., et al., 2018. A review on the applications of image logs in structural analysis and sedimentary characterization. Mar. Petrol. Geol. 95, 139–166. https://doi.org/10.1016/j.marpetgeo.2018.04.020.
Lai, J., Li, D., Wang, G., et al., 2019. Earth stress and reservoir quality evaluation in high and steep structure: the Lower Cretaceous in the Kuqa Depression, Tarim Basin, China. Mar. Petrol. Geol. 101, 43–54. https://doi.org/10.1016/j.marpetgeo.2018.11.036.
Lai, J., Wang, S., Zhang, C., et al., 2020. Spectrum of pore types and networks in the deep cambrian to lower ordovician dolostones in tarim basin, China. Mar. Petrol. Geol. 112, 104081. https://doi.org/10.1016/j.marpetgeo.2019.104081.
Lai, J., Chen, K., Xin, Y., et al., 2021a. Fracture characterization and detection in the deep Cambrian dolostones in the Tarim Basin, China: insights from borehole image and sonic logs. J. Petrol. Sci. Eng. 196, 107659. https://doi.org/10.1016/j.petrol.2020.107659.
Lai, J., Liu, S., Xin, Y., Wang, S., Xiao, C., Song, Q., Chen, X., Wang, G., Qin, Z., Ding, X., 2021b. Geological-petrophysical insights in the deep Cambrian dolostone reservoirs in Tarim Basin, China. AAPG Bulletin 105 (11), 2263–2296.
Lee, H.P., Olson, J.E., Holder, J., et al., 2015. The interaction of propagating opening mode fractures with preexisting discontinuities in shale. J. Geophys. Res. Solid Earth 120 (1), 169–181. https://doi.org/10.1002/2014JB011358.
Li, L.H., Huang, B.X., Li, Y.Y., et al., 2018. Multi-scale modeling of shale laminas and fracture networks in the yanchang formation, southern ordos basin, China. Eng. Geol. 243, 231–240. https://doi.org/10.1016/j.enggeo.2018.07.010.
Li, C., Zhao, L., Liu, B., et al., 2021. Origin, distribution and implications on production of bedding-parallel fractures: a case study from the Carboniferous KT-I Formation in the NT oilfield, Precaspian Basin, Kazakhstan. J. Petrol. Sci. Eng. 196, 107655. https://doi.org/10.1016/j.petrol.2020.107655.
Liu, B., Sun, J., Zhang, Y., et al., 2021. Reservoir space and enrichment model of shale oil in the first member of Cretaceous Qingshankou Formation in the Changling sag, southern Songliao Basin, NE China. Petrol. Explor. Dev. 48 (3), 1–16. https://doi.org/10.1016/S1876-3804(21)60049-6.
Liu, B., Bechtel, A., Sachsenhofer, R.F., et al., 2017. Depositional environment of oil shale within the second member of permian Lucaogou formation in the santanghu basin, northwest China. Int. J. Coal Geol. 175, 10–25. https://doi.org/10.1016/j.coal.2017.03.011.
Liu, C., Liu, K., Wang, X., et al., 2019. Chemo-sedimentary facies analysis of fine-grained sediment formations: an example from the Lucaogou Fm in the Jimusar sag, Junggar Basin, NW China. Mar. Petrol. Geol. 110, 388–402. https://doi.org/10.1016/j.marpetgeo.2019.06.043.
Liu, D., Zhang, C., Pan, Z., et al., 2020. Natural fractures in carbonate-rich tight oil reservoirs from the Permian Lucaogou Formation, southern Junggar Basin, NW China: insights from fluid inclusion microthermometry and isotopic geochemistry. Mar. Petrol. Geol. 119, 104500. https://doi.org/10.1016/j.marpetgeo.2020.104500.
Liang, M., Wang, Z., Zhang, Y., et al., 2021. Experimental investigation on gas permeability in bedding shale with brittle and semi-brittle deformations under triaxial compression. J. Petrol. Sci. Eng. 196, 108049. https://doi.org/10.1016/j.petrol.2020.108049.
McGinnis, R.N., Ferrill, D.A., Morris, A.P., et al., 2017. Mechanical stratigraphic controls on natural fracture spacing and penetration. J. Struct. Geol. 95, 160–170. https://doi.org/10.1016/j.jsg.2017.01.001.
Momeni, A., Rostamia, S., Hashemi, S., et al., 2019. Fracture and fluid flow paths analysis of an offshore carbonate reservoir using oil-based mud images and petrophysical logs. Mar. Petrol. Geol. 109, 349–360. https://doi.org/10.1016/j.marpetgeo.2019.06.021.
Mohammed, I., Olayiwola, T.O., Alkathim, M., et al., 2021. A review of pressure transient analysis in reservoirs with natural fractures, vugs and/or caves. Petrol. Sci. 18, 154–172. https://doi.org/10.1007/s12182-020-00505-2.
Nelson, R.A., 1985. Geologic Analysis of Naturally Fractured Reservoirs. Gulf Publishing, Houston, Texas, p. 320.
Nian, T., Wang, G., Xiao, C., et al., 2016. The in situ stress determination from borehole image logs in the Kuqa Depression. J. Nat. Gas Sci. Eng. 34, 1077–1084. https://doi.org/10.1016/j.jngse.2016.08.005.
Nian, T., Wang, G., Song, H., 2017. Open tensile fractures at depth in anticlines: a case study in the Tarim basin, NW China. Terra. Nova 29 (3), 183–190. https://doi.org/10.1111/ter.12261.
Nian, T., Jiang, Z., Wang, G., et al., 2018. Characterization of braided river-delta facies in the Tarim Basin Lower Cretaceous: application of borehole image logs with comparative outcrops and cores. Mar. Petrol. Geol. 97, 1–23. https://doi.org/10.1016/j.marpetgeo.2018.06.024.
Nian, T., Wang, G., Tan, C., et al., 2021. Hydraulic apertures of barren fractures in tight-gas sandstones at depth: image-core calibration in the lower cretaceous Bashijiqike Formation, Tarim Basin. J. Petrol. Sci. Eng. 196, 108016. https://doi.org/10.1016/j.petrol.2020.108016.
Niu, H., Liu, S., Lai, J., et al., 2020. In-situ stress determination and fracture characterization using image logs. Energy Science and Engineering 8, 476–489. https://doi.org/10.1002/ese3.529.
Price, N.J., 1966. Fault and Joint Development in Brittle and Semi-brittle Rock. Pergamon Press, Oxford, p. 176.
Rajabi, M., Sherkati, S., Bohloli, B., et al., 2010. Subsurface fracture analysis and determination of in-situ stress direction using FMI logs: an example from the Santonian carbonates (Ilam Formation) in the Abadan Plain, Iran. Tectonophysics 492 (1–4), 192–200. https://doi.org/10.1016/j.tecto.2010.06.014.
Strijker, G., Bertotti, G., Luthi, S.M., 2012. Multi-scale fracture network analysis from an outcrop analogue: a case study from the Cambro-Ordovician clastic succession in Petra, Jordan. Mar. Petrol. Geol. 38 (1), 104–116. https://doi.org/10.1016/j.marpetgeo.2012.07.003.
Swanson, S.K., 2007. Lithostratigraphic controls on bedding-plane fractures and the potential for discrete groundwater flow through a siliciclastic sandstone aquifer, southern Wisconsin. Sediment. Geol. 197, 65–78. https://doi.org/10.1016/j.sedgeo.2006.09.002.
Tang, J., Wu, K., Zeng, B., et al., 2018. Investigate effects of weak bedding interfaces on fracture geometry in unconventional reservoirs. J. Petrol. Sci. Eng. 165, 992–1009. https://doi.org/10.1016/j.petrol.2017.11.037.
Wang, C., Zhang, B., Hu, Q., et al., 2019. Laminae characteristics and influence on shale gas reservoir quality of lower Silurian Longmaxi Formation in the Jiaoshiba area of the Sichuan Basin, China. Mar. Petrol. Geol. 109, 839–851. https://doi.org/10.1016/j.marpetgeo.2019.06.022.
Wang, Y., Cao, J., Tao, K., et al., 2020a. Reevaluating the source and accumulation of tight oil in the middle permian Lucaogou formation of the Junggar Basin, China. Mar. Petrol. Geol. 117, 104384. https://doi.org/10.1016/j.marpetgeo.2020.104384.
Wang, G., Lai, J., Liu, B., et al., 2020b. Fluid property discrimination in dolostone reservoirs using well logs. Acta Geol. Sin. 94 (3), 831–846. https://doi.org/10.1111/1755-6724.14526.
Weng, X., Chuprakov, D., Kresse, O., et al., 2018. Hydraulic fracture-height containment by permeable weak bedding interfaces. Geophysics 83 (3), MR137–MR152. https://doi.org/10.1190/geo2017-0048.1.
Wilson, M.E.J., Lewis, D., Yogi, O., et al., 2013. Development of a Papua New Guinean onshore carbonate reservoir: a comparative borehole image (FMI) and petrographic evaluation. Mar. Petrol. Geol. 44, 164–195. https://doi.org/10.1016/j.marpetgeo.2013.02.018.
Wilson, T.H., Smith, V., Brown, A., 2015. Developing a model discrete fracture network, drilling, and enhanced oil recovery strategy in an unconventional naturally fractured reservoir using integrated field, image log, and three-dimensional seismic data. AAPG (Am. Assoc. Pet. Geol.) Bull. 99 (4), 735–762. https://doi.org/10.1306/10031414015.
Xu, C., Gehenn, J.M., Zhao, D., et al., 2015. The fluvial and lacustrine sedimentary systems and stratigraphic correlation in the Upper Triassic Xujiahe Formation in Sichuan Basin, China. AAPG (Am. Assoc. Pet. Geol.) Bull. 99 (11), 2023–2041. https://doi.org/10.1306/07061514236.
Xu, S., Gou, Q., Hao, F., et al., 2020. Multiscale faults and fractures characterization and their effects on shale gas accumulation in the Jiaoshiba area, Sichuan Basin, China. J. Petrol. Sci. Eng. 189, 107026. https://doi.org/10.1016/j.petrol.2020.107026.
Yawar, Z., Schieber, J., 2017. On the origin of silt laminae in laminated shales. Sediment. Geol. 360, 22–34. https://doi.org/10.1016/j.sedgeo.2017.09.001.
Zazoun, R.S., 2013. Fracture density estimation from core and conventional well logs

data using artificial neural networks: the Cambro-Ordovician reservoir of Mesdar oil field, Algeria. J. Afr. Earth Sci. 83, 55–73. https://doi.org/10.1016/j.jafrearsci.2013.03.003.

Zeng, L., Li, X., 2009. Fractures in sandstone reservoirs with ultra-low permeability: a case study of the upper triassic yanchang formation in the ordos basin, China. AAPG (Am. Assoc. Pet. Geol.) Bull. 93 (4), 461–477. https://doi.org/10.1306/09240808047.

Zeng, L., Lyu, W., Li, J., et al., 2016. Natural fractures and their influence on shale gas enrichment in Sichuan Basin, China. J. Nat. Gas Sci. Eng. 30, 1–9. https://doi.org/10.1016/j.jngse.2015.11.048.

Zhang, C., Zhu, D., Luo, Q., et al., 2017. Major factors controlling fracture development in the Middle Permian Lucaogou Formation tight oil reservoir, Junggar Basin, NW China. J. Asian Earth Sci. 146, 279–295. https://doi.org/10.1016/j.jseaes.2017.04.032.

Zhang, R.H., Wang, K., Zeng, Q.L., et al., 2021. Effectiveness and petroleum geological significance of tectonic fractures in the ultra-deep zone of the Kuqa foreland thrust belt: a case study of the Cretaceous Bashijiqike Formation in the Keshen gas field. Petrol. Sci. 18, 728–741. https://doi.org/10.1007/s12182-021-00567-w.

Zhang, S., Cao, Y., Liu, K., et al., 2019. Characterization of lacustrine mixed fine-grained sedimentary rocks using coupled chemostratigraphic-petrographic analysis: a case study from a tight oil reservoir in the Jimusar Sag, Junggar Basin. Mar. Petrol. Geol. 99, 453–472. https://doi.org/10.1016/j.marpetgeo.2018.10.039.

Zhang, Y., He, Z., Jiang, S., et al., 2019. Fracture types in the lower Cambrian shale and their effect on shale gas accumulation, Upper Yangtze. Mar. Petrol. Geol. 99, 282–291. https://doi.org/10.1016/j.marpetgeo.2018.10.030.